LAWRENCE
LIVERMORE
NATIONAL
LABORATORY

LLNL-JRNL-840405

Aging of UV Curable PDMS Developed for Large-scale High Viscosity Stereolithography

H. Song, N. A. Rodriguez, J. Oakdale, E. B Duoss, R. Crawford, C. Seepersad

September 28, 2022

Polymer Degradation and Stability

Disclaimer

Aging of UV Curable PDMS Developed for Large-scale, High Viscosity Stereolithography

Hongtao Song[1], Nicholas A. Rodriguez[1,2], James S. Oakdale[2], Eric B. Duoss[2], Richard H. Crawford[1], Carolyn C. Seepersad[1,3]

Key Words: Aging Research, Polydimethylsiloxane, Hydrosilylation, Stereolithography, Additive Manufacturing

Abstract

Polydimethylsiloxane (PDMS) elastomers are silicone rubbers that find widespread application in both academic and industrial settings. This study investigates the use of photosensitive platinum catalysts for UV-activated hydrosilylation of PDMS, which enables the additive manufacturing of PDMS objects through techniques such as stereolithography. Specifically, this study focuses on understanding the aging behavior of Pt-catalyzed, UV-curable PDMS samples, including their mechanical behavior under thermal and UV-accelerated aging conditions. The results show that the Pt-catalyzed, UV-curable PDMS introduced in this research is 'under-cured' after being printed and will slowly evolve over time resulting in increased stiffness and decreased elongation, likely due to the formation of additional crosslinks. FTIR spectroscopy indicates that no new chemical bonds or functional groups are generated through the aging process, suggesting that no thermal degradation or polymer chain scissions occur in the polymer matrix. Overall, this PDMS formulation exhibits greater mechanical strength and significantly less reduction in strength with aging, compared with the commonly used, UV-curable thiol-ene PDMS.

[1] Walker Department of Mechanical Engineering, The University of Texas at Austin, Austin, TX 78712
[2] Lawrence Livermore National Laboratory, Livermore, CA, 94550
[3] Corresponding Author: ccseepersad@mail.utexas.edu

1. Introduction

PDMS offers unique material properties: excellent mechanical properties, optical transparency, low toxicity and biocompatibility, permeability to gas, and impermeability to water (Cong & Pan, 2008; Liravi & Toyserkani, 2018). As it is relatively inexpensive, PDMS is a popular choice for optical (Schneider, Draheim, Kamberger, & Wallrabe, 2009), electronic (Tian et al., 2017), bio-medical (Holländer et al., 2018), soft lithography, and microfluidic application (Raj M & Chakraborty, 2020). Various additive manufacturing methods have been developed to 3D print silicone materials, including direct ink writing (DIW), material jetting, and stereolithography (SLA) (Liravi & Toyserkani, 2018). Direct ink writing is capable of depositing both low and high viscosity liquid (up to 6×10^7 mPa*s viscosity with a shear-thinning behavior), but the minimal feature size and volumetric throughput are limited by the nozzle size (Murphy & Atala, 2014). Material jetting offers better resolution, but the highest viscosity it can accommodate is two orders of magnitude lower than DIW (Yang et al., 2013). Both approaches show limited abilities to print large volume structures with fine features.

Stereolithography, on the other hand, offers fine features and high material throughput. The printing volume is also easy to scale. However, most commercial SLA machines operate with low viscosity resins, which is not ideal for printing elastomers. Elastomers are often composed of high molecular weight monomers compounded with reinforcing filler particles to achieve high ultimate strength and high elongation at break. As a result, elastomer resins often have higher viscosities and require light systems with higher intensity than those typically used in SLA machines (Al-Turaif, 2010; Xiao et al., 2018). We have built a novel large-scale, high-viscosity stereolithography system to print high-viscosity silicone, as shown in Figure 1 (a). This machine features a bottom-

up design with an imaging area of 370 mm * 300 mm, and a resin dispensing system that is capable of processing resins with a maximum viscosity of 200,000 Pa*s. To fulfill the requirement for high intensity light, the machine includes a novel light patterning system that incorporates two wire grid polarizers (WGPs) with a liquid crystal display (LCD) monitor. Combined with a high-power UV LED array as the light source, this system is capable of outputting a maximum intensity of ~100 mW/cm^2 at a wavelength of 385 nm over the entire print area (N. A. Rodriguez et al., 2022). Furthermore, a roll-to-roll variable tensioning system was developed to reduce the separation force induced when the printed layer is separated from the vat floor after each layer and thereby avoid damaging small features (Song et al., 2021). The existence of this printer motivates the investigation of new formulations of PDMS resins with improved aging behavior, even if the enhanced properties require higher viscosity resins and greater light intensities for curing.

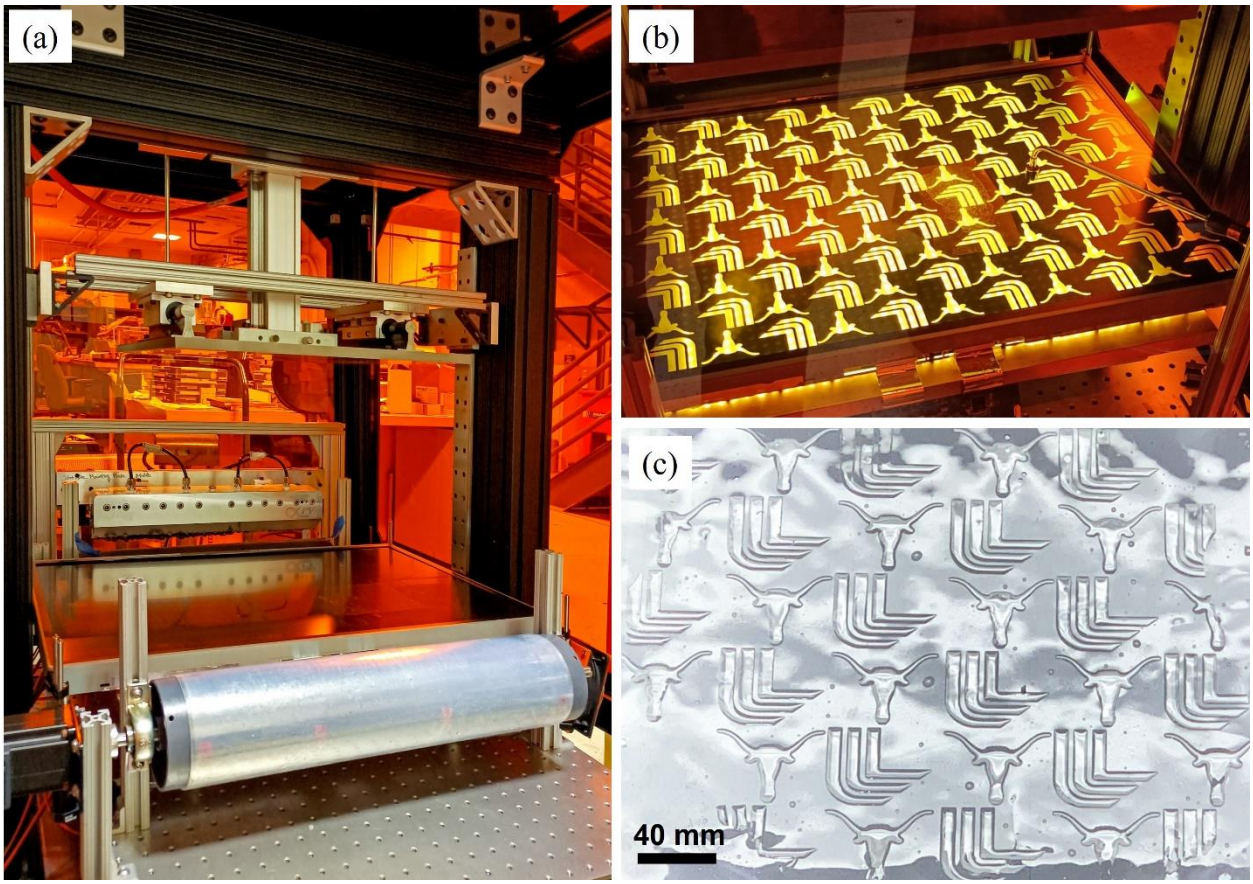

*Figure 1 (a) the large-scale, high viscosity stereolithography printer, (b) the light patterning system displaying a checkboard pattern of longhorn and LLNL logos, (c) printed single layer pattern with a dimension of 300 mm * 250 mm*

Years of research have been devoted to formulating PDMS for stereolithography. A common approach involves the use of free radical polymerization as the primary cure mechanism. Free radical systems usually contain thiol-ene, acrylate, thiol-acrylate, or methacrylated functional groups (N. Rodriguez et al., 2021; Sirrine et al., 2018; Thrasher, Schwartz, Boydston, & interfaces, 2017; Wallin et al., 2017). Spatially controlled actinic radiation generates highly reactive free radicals via excitation of photoinitiators, and the localized radicals drive the formation of PDMS networks (i.e., curing). (Dendukuri et al., 2008).

Photoinitiated thiol-ene reaction, as one of the click chemistries, has been widely adopted in stereolithography for its printability. The thiol-ene polymerization can be initiated with local and temporal exposure to UV radiation, resulting in a rapid gelation process with a high conversion rate, high resolution and accuracy (Sycks, Wu, Park, & Gall, 2018; H. Xiang et al., 2019). The chemistry of the thiol-ene polymerization is shown in Figure 2 (a). However, reactive functional groups, such as enes and thiols, are usually not fully converted during free-radical polymerization (Zheng, Zlatin, Selvaganapathy, & Brook, 2018). The conversion rate of these functional group ranges between 63 and 86% under curing parameters common for SLA. Over time, remaining functional groups may continue to react, causing chemical and mechanical changes to the bulk material. The aging of the acrylated PDMS has been shown to result in a decline of mechanical properties, accompanied by discoloration (Hopf et al., 2016). Similarly, our preliminary aging experiment also observed significant aging of the thiol-ene PDMS (as shown in Figure 3 (a) and (c); details of the test can be found in the supplemental material, Table S1). With only 24 hours of UV aging, the tensile strength decreased from 2.65 MPa to 1.20 MPa, and the elongation dropped

from more than 900% to 220% with a corresponding change of color. The thiol-ene PDMS is extremely sensitive to UV illumination, which means it is not suitable for any application that may receive UV illumination in the field.

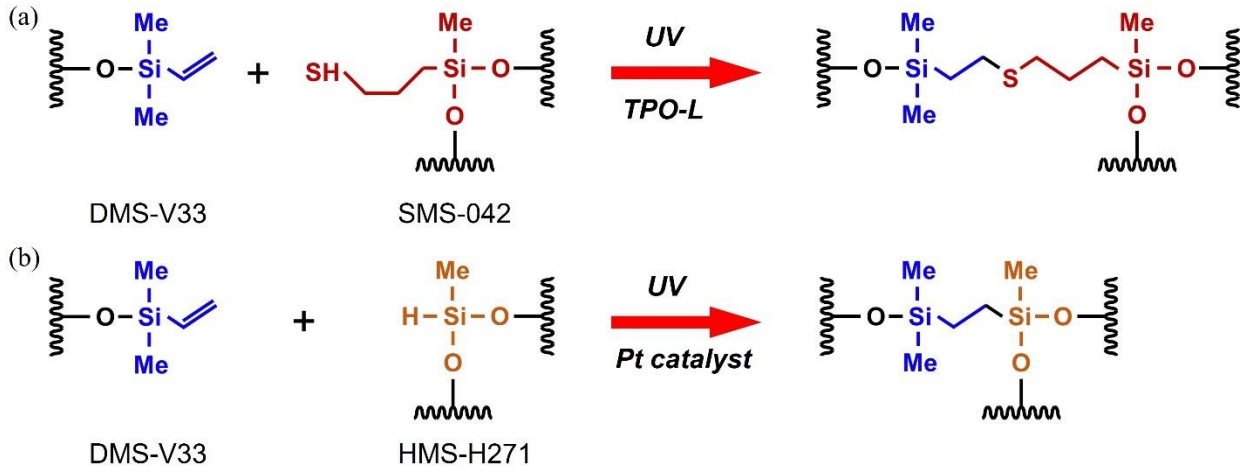

Figure 2 The crosslinking mechanism of different UV-curable PDMS. (a) Crosslinking mechanism of the thiol-ene PDMS formulation, (b) Crosslinking mechanism of the Pt-catalyzed, UV-curable PDMS formulation.

Hydrosilylation, on the other hand, is a widely used reaction in industry to polymerize silicones (Lukin, Kuchkaev, Sukhov, Bekmukhamedov, & Yakhvarov, 2020). Here, unsaturated carbon-carbon double bonds (C=C), usually vinyl functionalized siloxane, react stoichiometrically with silicon hydride groups (Si-H) in the presence of a catalyst (usually platinum complexes), to generate Si-CH_2-CH_2-Si linkages (Bhagat, Jothimuthu, & Papautsky, 2007; Hayashi & Yamasaki, 2007). Typically, hydrosilylation proceeds at or above room temperature in the presence of a platinum catalyst such as Karstedt's catalyst, and this process is referred to as thermal-hydrosilylation to distinguish these systems from their UV-cure analogs. Organo-platinum complexes have been developed to catalyze hydrosilylation upon actinic radiation (Oxman & Boardman, 1992, 2002). Photosensitive platinum complexes, such as platinum (II) bis(acetylacetonate) [$Pt(acac)_2$], and trimethyl(methylcyclopentadienyl) platinum (IV) [(Me-Cp)$Pt(Me)_3$] (Fry & Neckers, 1996; Mayer, Burget, Mignani, & Fouassier, 1996; Xi et al., 2019),

are triggered by UV irradiation. We are actively developing actinic Pt-catalyzed PDMS systems for SLA and related additive manufacturing methodologies and the chemistry of the actinic Pt catalyzed formulation is shown in Figure 2 (b). Compared to the thiol-ene formulation, the Pt-catalyzed, UV-curable PDMS samples showed significantly better UV aging properties. As shown in Figure 3 (b) and (d), there is not a significant decrease in the tensile strength or change in color with UV aging. The stiffness of the sample increased slightly, possibly due to the continuation of the crosslinking reaction.

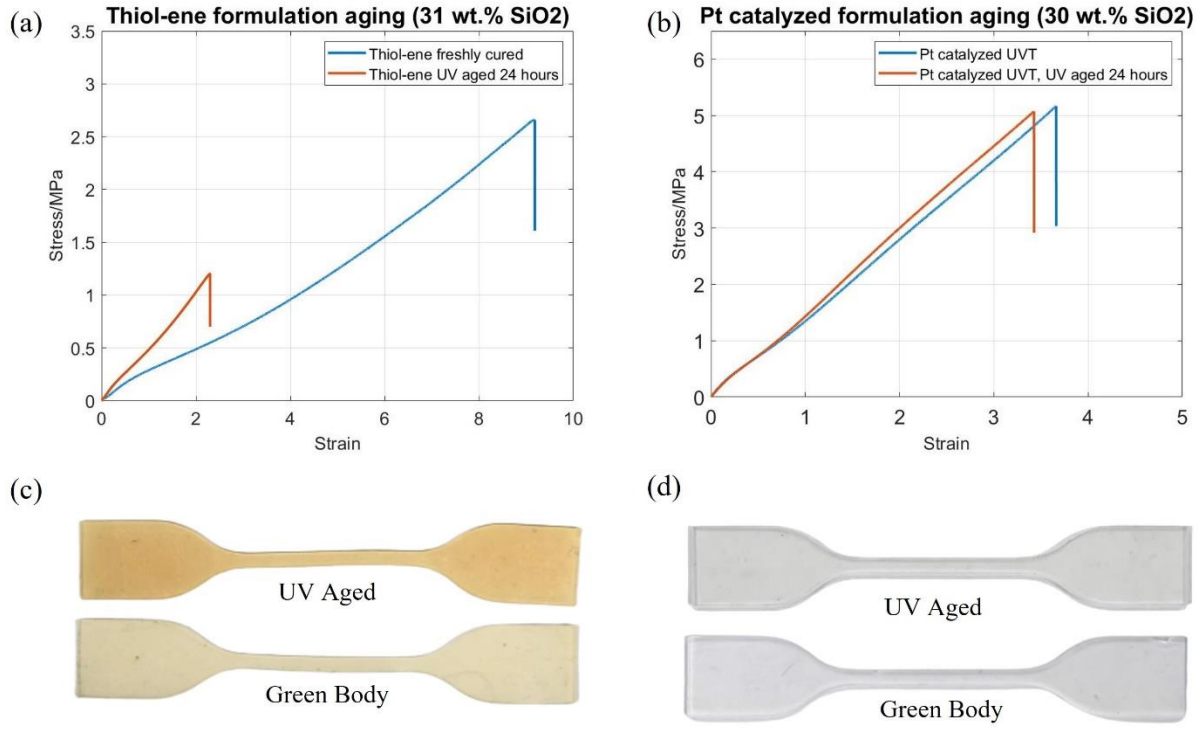

Figure 3 Aging comparison between thiol-ene PDMS and Pt-catalyzed PDMS (a) Stress-strain curves of the thiol-ene PDMS with 15 wt.% silica nanoparticles as the reinforcement, (b) Stress-strain curves of the Pt-catalyzed PDMS with 30 wt.% silica nanoparticles as the reinforcement, (c) color of the thiol-ene PDMS samples, top: UV aged sample, bottom: green body; (d) color of the Pt-catalyzed PDMS samples, top: UV aged sample, bottom: green body.

Current research on the aging of Pt-catalyzed, UV curable PDMS is limited. Cai et.al. researched the broadband UV weathering effects on two commercially available Pt-catalyzed PDMS formulations (Cai, Miller, Tappan, Dauskardt, & Cells, 2016), with an intensity equivalent to 1100

times solar concentration and a peak wavelength at 320 nm. The high UV intensity and high aging temperature (at 110 °C) resulted in oxidation of the Si-CH_3 groups and generation of Si-O-Si linkages. The resultant polymer showed significantly increased adhesion energy, but no other mechanical property was reported. Masson et.al. conducted UV aging research on three commercially available room-temperature vulcanized (RTV) silicone formulations. The result showed increased storage modulus, contact angle and crystallization temperature, and reduced weight after UV aging (Masson, Collins, Riahinezhad, Lopez-Carreon, & Johansen, 2022). Murano and his colleagues conducted UV aging research on a commercial PDMS insulator that has served in the field for 12 years under normal sunlight (Munaro et al., 2019). Nuclear Magnetic Resonance (NMR) and Dynamical Mechanical Thermal Analysis (DMTA) testing results indicate that the crosslinking reaction continued over time in the polymer matrix, resulting in lower melting temperature, more heterogeneous crosslinked networks, and a more rigid polymer. However, no mechanical property data or change of chemistry was reported in this research. Other research focused on the effect of UV illumination on PDMS surface properties, such as surface energy and hydrophobic behavior. UV illumination is used as a surface treatment to modify the surface of the PDMS resin to increase adhesion and improve the wetting of aqueous solvents (Eddington, Puccinelli, & Beebe, 2006).

There have been many studies on the thermal degradation of PDMS, which typically investigate kinetic aspects of degradation reactions (Hanu, Simon, Cheng, & stability, 2006) under high temperatures (usually over 250 °C). Since silicone is composed of siloxane bonds (Si-O-Si) with a higher binding energy than C-C bonds in organic polymers, it exhibits a superior thermal durability (Mata, Fleischman, & Roy, 2005). At temperatures greater than 250 °C, thermal degradation involves breaking of Si-CH_3 groups in the main chain and generation of Si-O-Si due

to oxidation, causing changes in mechanical properties and weight (Kaneko et al., 2019; Shimada et al., 2014). The thermal degradation at lower temperatures, especially under 150 °C is limited. Xiang and his colleagues conducted high-temperature thermal aging research on a commercial PDMS formulation reinforced with fumed silica nanoparticle (K. Xiang et al., 2012). This research focused on the change of elongation and compression behavior under high temperatures up to 250 °C and revealed that thermal aging of PDMS is strongly temperature dependent. This research did not report any changes in mechanical properties, such as strength and modulus. Other research has been conducted on the thermal aging process to tailor the desired mechanical properties (swelling ratio, hydrophobic behavior, etc.), but they do not report on the change of chemistry (M. Liu, Sun, & Chen, 2009).

None of the current studies report aging of Pt-catalyzed, UV-cured silicone under both UV and thermal aging conditions. In this research, the aging behavior of the Pt-catalyzed, UV-curable PDMS was investigated. Both UV and thermal aging tests were conducted on samples obtained through a UV-initiated hydrosilylation process. Mechanical properties, which include tensile strength, Young's modulus, elongation at break, hardness, and the swelling ratio were tested before and after aging. FTIR spectroscopy was conducted on both the freshly cured and aged samples to explore changes in chemistry. The results enhance our understanding of how mechanical properties of PDMS change under UV and thermal stress and, ultimately, ensure the long-term performance of end products fabricated from Pt-catalyzed, UV-curable PDMS.

2. Material and Method

2.1 Resin formulations and curing conditions

UV curable resin systems consist of 97.8 phr (the mass part of filler per hundred mass parts of rubber) vinyl terminated polydimethylsiloxane (DMS-V33, Gelest, Inc.) mixed with 2.2 phr of hydride functional polydimethylsiloxane (HMS-H271, Gelest, Inc.). 100 ppm (trimethyl)pentamethylcyclopentadienylplatinum(IV) (Cp*$PtMe_3$, Strem Chemicals, Inc.) was added as a catalyst, followed by 300 ppm of 9,10-diethoxyanthracene (Anthracure, BOC Sciences, Inc.) as a sensitizer. Mixing was conducted with a vacuum centrifugal mixer (Thinky ARV-310) operating at 2000 rpm for 1 min. Finally, 43 phr of fumed silica nanoparticles (SIS6962.0, Gelest, Inc.) were added via centrifugal mixing, resulting in a concentration of 30 wt.%.

The catalyst, Cp*$PtMe_3$ can be activated by UV radiation or in a high-temperature environment (>100 °C). In this study, three curing conditions were used to prepare the aging samples, as listed in Table 1. The UV stands for UV curing only, which received a dose of ultraviolet illumination of 60 s under 250 mW/cm^2 with the wavelength of 405 nm. This curing condition is equivalent to the dose of ultraviolet illumination the green body received in the previously described SLA printer. The UVT stands for UV curing with the same dose of ultraviolet illumination as the UV group, plus thermal post-curing at 135 ℃ for 12 hours. Since thermal post-curing at temperatures over 120 ℃ is common for Pt-catalyzed silicones to achieve the full mechanical properties, UVT represents the curing condition of end products. Finally, a group of samples that were thermally cured only are noted as the T group, which were cured at 135 ℃ for 12 hours is added for comparison.

Table 1 Conditions to cure PDMS

Group Notation	**UV illumination (405 nm)**	**Thermal curing (135 °C)**
UV	60 s @ 250 mW/cm^2	-
UVT	60 s @ 250 mW/cm^2	12 hours

T	-	12 hours

2.2 Mechanical Properties Test

The mechanical tests focused on four properties: tensile strength S_{ut}, Young's Modulus E, elongation at break γ_{ut}, and Shore A hardness.

Tensile testing followed the ASTM D412-15 testing standard with type D specimen. The dimensions of type D specimen are shown in Figure S1 in the supplemental material. Samples were prepared by first spreading liquid resin with a thickness of 1.5 mm on an aluminum panel with the help of a doctor blade. Next, the resin was cured under UV illumination or in a forced convection oven, depending on the required curing method. Additional thermal post-curing was added to the UVT group. After the curing process was complete, the cured PDMS sheet was cut into type D specimens with a dumbbell die cutter.

The tensile strength, Young's modulus, and elongation were tested on a universal testing machine (Instron 3345) with a 50 N load cell (Instron Model 2519-50N, 50 N capacity). The load rate was fixed at 0.2 mm/s to eliminate viscoelastic behavior. For each group of samples, at least three specimens were tested. The hardness test followed the ASTM D2240-15 testing standard using a portable Shore A durometer. The hardness tests were repeated five times at different locations, and the average value was computed as the hardness.

2.3 UV aging experiment

UV aging followed ASTM G154-16 standard. Tensile specimens cut from cured PDMS sheets were placed in a custom-built UV aging chamber with two 20 W UVA 340 fluorescent light tubes as the UV light source. The irradiance spectrum of a UVA 340 lamp matches the spectrum of sunlight under 400 nm wavelength, as shown in the supplemental material (Fig.S2), which makes them an ideal light source to mimic UV aging in practice. The UV irradiance each specimen received was fixed at 0.89 W/(m^2*nm), as required by the ASTM G154-16 standard. The exposure cycle was set to 12 hours: 8 hours of UV illumination at 60 (±3) °C black panel temperature, and 4 hours of condensation at 50 (±3) °C black panel temperature. The aging time was set to 2 weeks, 4 weeks, 6 weeks, 8 weeks, and 12 weeks. A group of tensile specimens was stored at room temperature and isolated from ambient light for up to 8 weeks as a control group.

2.4 Thermal aging experiment

The thermal aging test followed ASTM D865-11 standard. The tensile specimens were aged in a forced convection oven. Each tensile specimen was isolated in a borosilicate glass tube and sealed with a cork to prevent oxidation. Each glass tube was covered with a sheet of aluminum foil to block ambient light. The aging time was set to 1 to 4 weeks, with the temperature set at 100 °C. According to ASTM F1980 accelerated aging standard, aging at 100 °C for 4 weeks is equivalent to 7500 days, or 20.54 years at room temperature.

2.5 Fourier-transform infrared spectroscopy (FTIR) test

FTIR tests were conducted on the uncured, green body and aged samples to evaluate changes in chemical bonds and functional groups. The tests were conducted on an Infinity Gold FTIR

(Thermo Mattson, Waltham, MA, USA), with the results recorded between 500 and 3000 cm^{-1} wavenumbers with a resolution of 2 cm^{-1} and averaged between 256 scans. At least five samples were tested for each group.

2.6 Compression test

Compression experiments were conducted on UV and UVT groups. The compression test followed ASTM 6147-97 standards. The liquid resin was spread and cured into a 6 mm thick sheet following the same curing conditions listed in section 2.1 and cut into 16 mm x 16 mm blocks. Blocks were compressed to 4 mm thickness in type B compression clamps, with the compression time set to 4 weeks. Compression sets were placed in the UV aging chambers, the forced convection oven as well as a light-tight chamber at room temperature. After 4 weeks, the thickness of each specimen was re-measured. The type B compression ratio C_B can be calculated by the following equation:

$$C_B = \frac{t_0 - t_i}{t_0 - t_n} \times 100 \quad (1)$$

Where t_0 is the original specimen thickness, t_i is the specimen thickness after testing and t_n is the spacer thickness or the specimen thickness during the test.

3. Results and Discussion

3.1 Mechanical Properties

The stress-strain curves of the freshly cured samples are plotted in Figure 4. As stated in Section 2, UVT stands for UV curing with thermal post cure, UV stands for UV curing only, and T stands for thermal curing only. The results show that the UVT samples have the highest strength and

stiffness with the lowest elongation, while the UV samples have the lowest tensile strength and stiffness with the highest elongation. This result showed that the thermal post-curing increased the tensile strength and stiffness of the material, but with a reduction in elongation.

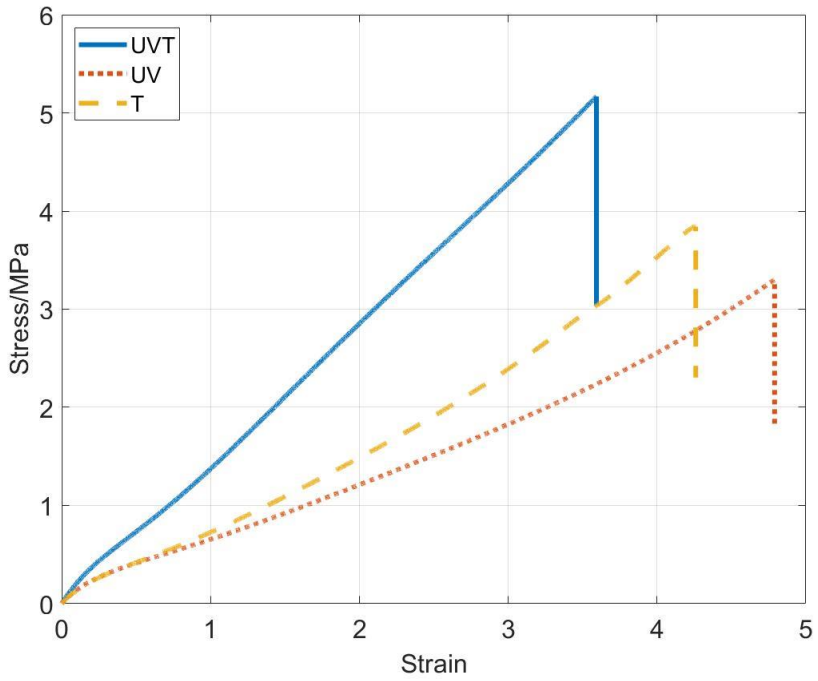

Figure 4 Stress-strain curves of the freshly cured tensile specimens (UVT: UV curing for 60 seconds with 405 nm UV and thermal post cure for 12 hours at 135 °C; UV: UV curing for 60 seconds with 405 nm UV; T: thermal curing for 12 hours at 135 °C)

The mechanical properties of aged UVT samples are plotted in Figure 5 (a). The tensile strength, S_{ut}, Young's modulus, E, and elongation at break, γ_{ut}, are plotted separately in each sub-figure. All the aging samples are noted by 'curing condition'_'aging condition'. For example, UVT_UV-aged stands for a sample that's cured under UVT curing condition, and aged under the UV aging condition that followed ASTM G154-16 standard. Thermally-aged stands for samples that are thermally aged that followed ASTM D865-11 standard. Room-temperature stands for samples that are stored in the stored at room temperature and isolated from ambient light as a control group. The tensile strength, S_{ut}, of the UVT_thermally-aged stayed relatively stable at ~ 5 MPa. The

Young's modulus, *E*, of the UVT_thermally-aged samples increased by 10% for the first 2 weeks, then stabilized at ~ 2.6 MPa. A similar trend is also observed for the UVT_UV-aged samples, where Young's modulus increased by 18% in first 4 weeks and stabilized between 2.6 and 2.7 MPa. The elongation of the UVT_UV- and UVT_thermally-aged samples, on the other hand, decreased by 25% in the first few weeks and then stabilized at ~ 300%. The general trend in mechanical properties of the UVT_UV- and UVT_thermally-aged samples are identical, with the UVT_thermally-aged samples reaching a stable state at a faster rate. The Young's modulus of the UVT_room-temperature-aged samples stays relatively stable over the entire 8 weeks of aging, at ~ 2.2 MPa. A slight decrease in elongation (8.8%) and tensile strength (9.8%) was observed. The Shore A hardness of the UVT samples generally increased from 43.4 to 46.8 regardless of the aging conditions, and the hardness of the aging samples has a positive correlation with Young's modulus (Figure S3(a)). Overall, the tensile strength of the UVT samples stays relatively stable over the duration of the aging experiments while Young's Modulus and elongation were observed to stabilize after a few weeks.

The mechanical properties of the aged UV samples are plotted in Figure 5(b). The tensile strength of all the aged samples increased over time. The tensile strength, S_{ut}, of the UV_UV- and UV_thermally-aged samples stabilized at 4.77 and 4.83 MPa, respectively. The changes in Young's modulus and elongation of UV group samples are similar to those observed in UVT group samples. For UV_UV-aged samples, Young's modulus increased by 52% after week 4, elongation decreased by 33% after week 6. For UV_thermally-aged samples, Young's modulus increased by 48% after week 1, elongation decreased by 37% after week 3. The Shore A hardness of the UV group samples increased from 39.7 to 46.4 after aging. The hardness of the aging samples also shows a positive correlation with Young's modulus (Figure S3(b)). The UV_room-temperature

samples also showed increased tensile strength, Young's modulus, and decreased elongation. This phenomenon may suggest that polymerization processes continue even without any additional light. The strength and stiffness of printed parts gradually increased and stabilized after ~4-6 weeks, in absence of post-print process. Post-curing, either via UV-light or exposure to elevated temperatures, accelerates the "aging" process, resulting in harder parts with higher tensile strength and stiffness. In the event that post-curing is not possible, these results suggest that UV-hydrosilylation UV-cured silicone elastomers should be allowed to 'age' for at least 4 weeks prior to end-use application.

When comparing the aging behavior of the UVT group and UV group samples, the mechanical properties of the samples at the end of the aging experiment are similar. Thermal aged samples reach peak Young's modulus in less than 2 weeks, while UV aged samples need at least 4 weeks. This phenomenon suggests that thermal aging induces a higher aging rate in both UV and UVT group samples. For the UVT group samples, thermal post-curing before the aging experiment is hypothesized to result in a relatively high degree of functional group conversion, which contributes to stable mechanical properties. For UV group samples, we hypothesize that the degree of functional group conversion is relatively lower and therefore aging conditions simple act as post-curing treatment to yield full mechanical performance.

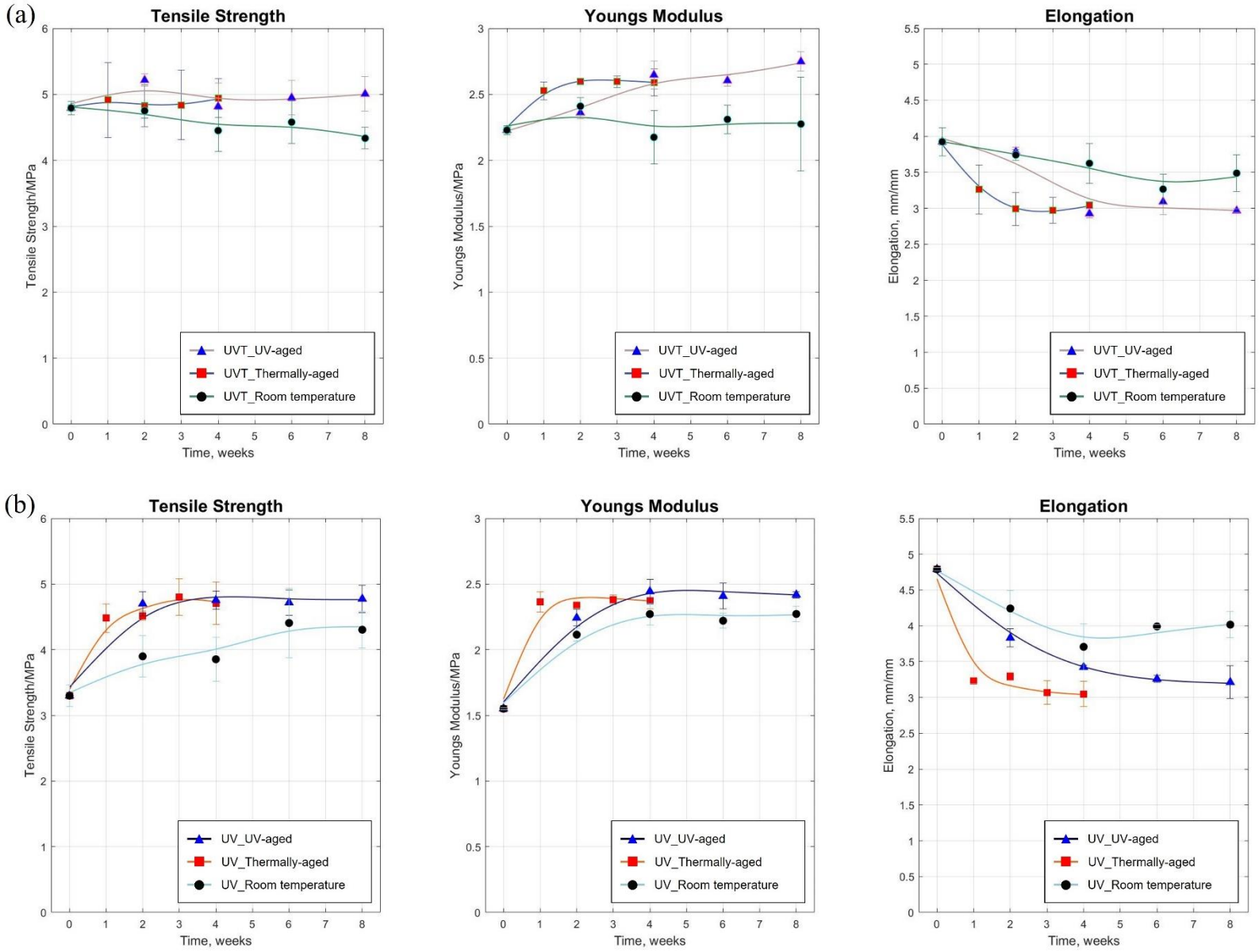
(a)
Tensile Strength
Tensile Strength/MPa
Time, weeks
UVT_UV-aged
UVT_Thermally-aged
UVT_Room temperature
Youngs Modulus
Youngs Modulus/MPa
Time, weeks
UVT_UV-aged
UVT_Thermally-aged
UVT_Room temperature
Elongation
Elongation, mm/mm
Time, weeks
UVT_UV-aged
UVT_Thermally-aged
UVT_Room temperature
(b)
Tensile Strength
Tensile Strength/MPa
Time, weeks
UV_UV-aged
UV_Thermally-aged
UV_Room temperature
Youngs Modulus
Youngs Modulus/MPa
Time, weeks
UV_UV-aged
UV_Thermally-aged
UV_Room temperature
Elongation
Elongation, mm/mm
Time, weeks
UV_UV-aged
UV_Thermally-aged
UV_Room temperature

Figure 5 Mechanical properties change under different aging conditions (a) UVT group (b) UV group

3.2 FTIR Analysis

FTIR spectra of the uncured resin, UV green body sample, 4 weeks UVT_thermal-aging, and 12 weeks UVT_UV-aging are shown in *Figure 6*. All of the samples showed signals at 786, 1006, 1063, 1260, and 2168 cm^{-1}. The broad peak between 750-865 cm^{-1}, and the peak at 1256 and 2965 cm^{-1}, are characteristic of the Si-CH_3 group (Wang, Lu, & Ma, 2019). The broad peak between 1000~1100 cm^{-1} indicates Si-O-Si (Wang et al., 2019). These chemical bonds are shared by both silicone rubber components, HMS-H271 and DMS-V33.

Previous studies use silane (Si-H, 2168 cm^{-1}, shown in Figure S4) and Si-CH=CH_2 (1400, 1600, and 3000 cm^{-1}) to monitor the degree of crosslinking, as the Si-H group reacts with the vinyl group during the curing process (i.e. hydrosilylation), resulting in reduced intensity at these peaks in cured samples (G. Liu, Kaspar, Reinold, Graczyk-Zajac, & Riedel, 2013; Lu & Li, 2016). However, the intensities of those signals are already very low in the HMS-H271 and DMS-V33 samples, and the intensities change of these peaks are negligible before and after the polymerization. Thus, both Si-H and Si-CH=CH_2 peaks cannot be used to monitor the degree of crosslinking in this study.

Si-H and Si-CH=CH_2 react to form a Si-CH_2-CH_2-Si bond in the cured samples. The board absorbance band between 1000 to 1150 cm^{-1} is composed of responses from multiple functional groups, including siloxane (Si-O-Si) at 1006 cm^{-1}. The Si-CH_2-CH_2-Si response appears as a shoulder, i.e. between 1060 and 1080 cm^{-1} (Wang et al., 2019). As shown in the zoom-in section in Figure 4 (a), the increased intensity of the shoulder peak suggests an increased response of the Si-CH_2-CH_2-Si signal and therefore increased degree of conversion. The average intensity of

shoulder peak between 1060 and 1080 cm^{-1} of each tested sample was calculated. We obtained the degree of functional group conversion through Equation 4 by setting the peak response between 1060 and 1080 cm^{-1} of the uncured sample as 0 %, and the peak response between 1060 and 1080 cm^{-1} of the UVT-T sample aged 4 weeks as 100 %:

$$I = \frac{i_{sp} - i_{uc}}{i_{UVT-T4} - i_{uc}} \times 100\% \quad (2)$$

where i_{sp} is the average intensity between 1060 and 1080 cm^{-1} of the sample, i_{uc} is the average intensity between 1060 and 1080 cm^{-1} of the uncured sample, i_{UVT-T4} is the average intensity between 1060 and 1080 cm^{-1} of the UVT sample after thermal aging for 4 weeks. The calculated degrees of conversion are shown in *Figure 6* (b):

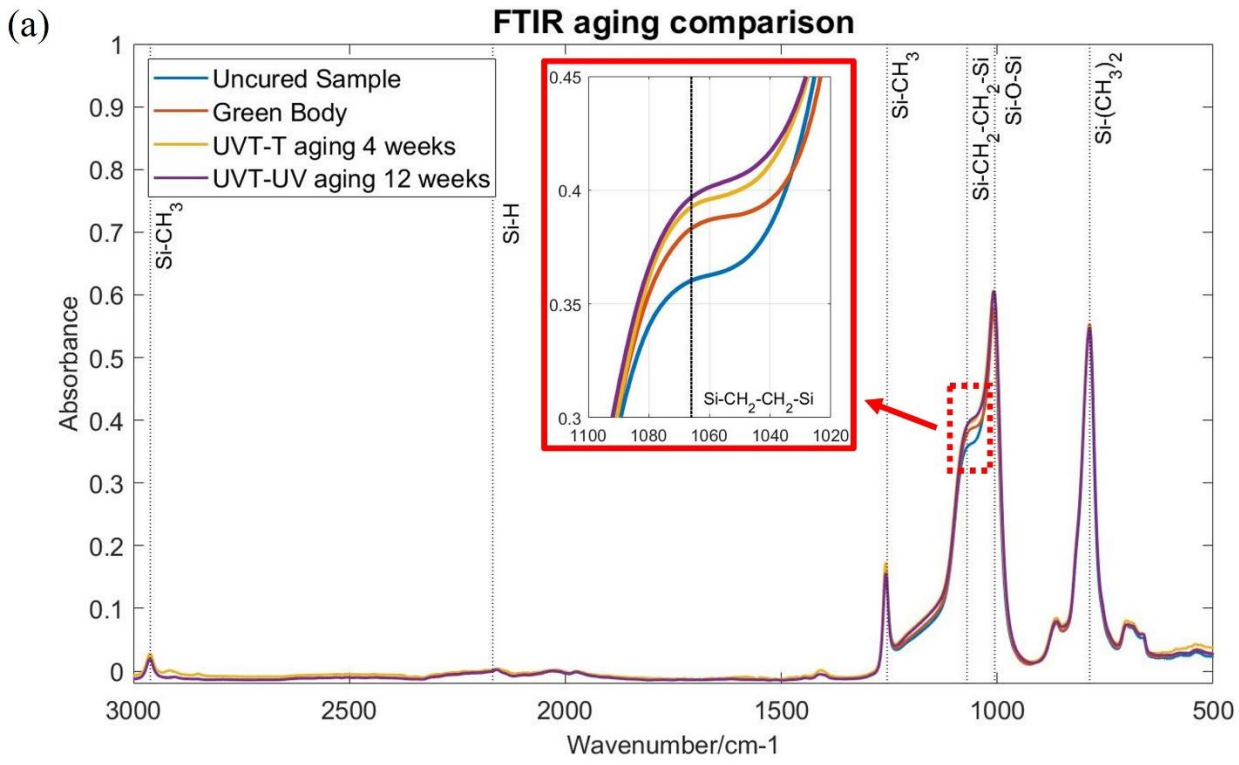

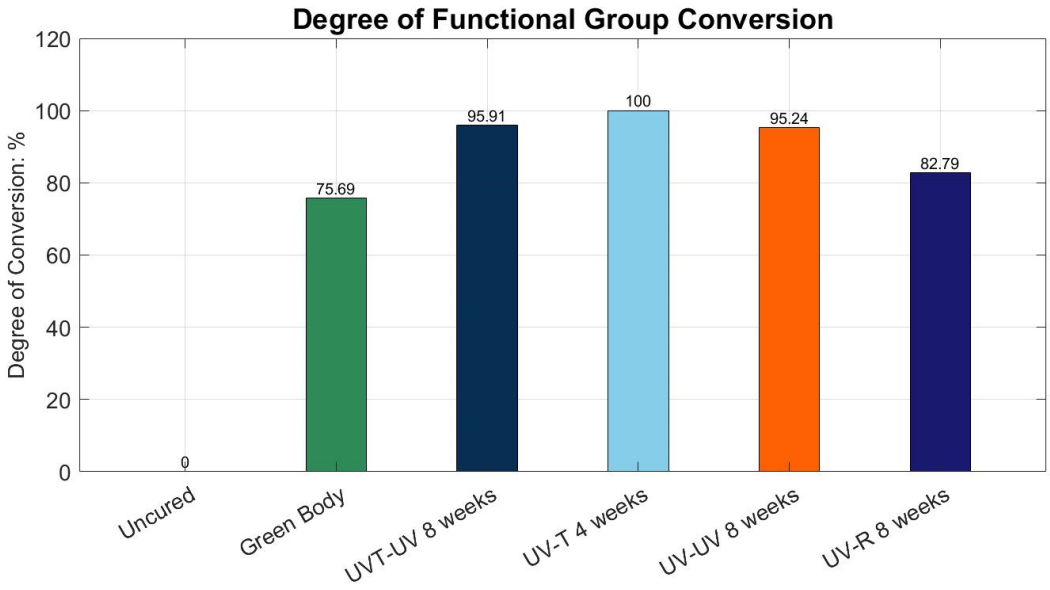

Figure 6 (a) FTIR spectra of the uncured sample, UV cured green body, UVT-T (thermal) aging for 4 weeks, UVT-UV-aging for 12 weeks and UV-R (room temperature in the dark) aging for 8 weeks; (b) Peak responses of tested specimens at 786, 1006 and 1056 cm^{-1}

Figure 6 (b) showed that the degree of functional group changes as the sample is aged. The green body sample has the lowest degree of conversion among all the polymerized samples, at 74.73%. The UV-R (room temperature aging) sample has a higher degree of conversion than the green body sample, which suggests that the crosslinking continues in the dark. UVT_UV-aged, UV_UV-aged, and UV_thermally-aged samples exhibit degrees of conversion greater than 94%, which means that the crosslinking process continued during the aging process, generating more Si-CH_2-CH_2-Si bonds, thereby increasing the degree of entanglement resulting in increased stiffness and decreased elongation, consistent with the mechanical data observed in *Figure 5*.

Looking at other peaks in Figure 6 (a), the intensity of peaks at 786 cm^{-1} and 1006 cm^{-1} are stable over the entire lifespan of the aging samples, indicating that the Si-O-Si and Si-$(CH_3)_2$ are unchanged over time. The Si-O-Si is the from the siloxane backbone of the silicone, as are the Si-$(CH_3)_2$ groups. The stable intensity of both chemical bonds suggests that the main monomer chains remained unchanged over the aging process. None of the aging methods affected the backbone of

the monomer, thus the changes in mechanical properties are related to other changes in the polymer. UVT_thermally-aged, UV_UV-aged, and UV_thermally-aged samples showed identical FTIR spectra as well as intensities of 786, 1006, 1060~1080 cm^{-1} peaks. The similarity of the FTIR spectra between thermally-aged samples and UV-aged samples suggests that the aging mechanisms are the same, which is the continuation of crosslinking. No new absorption peaks were discovered in any of the aged samples, meaning that under current aging conditions, there are no new chemical bonds or functional groups generated through the aging process. Combined with the swelling test result shown in Figure S5, there is no evidence that degradation or chain scission occurred in any of the aging samples.

3.3 Compression set test

Compression set tests were conducted only on UV and UVT samples. The thickness of each sample was measured before and after the compression test and the compression ratio was calculated using Equation (1). The calculated compression ratios are listed in Figure 7. All tested samples showed decreased thickness after compression. Generally, the UV samples exhibited a higher compression set compared to the UVT analogs. This result is likely a direct consequence of having a lower initial degree of crosslinking. The continuation of curing during the compression experiment likely locks polymer chains in their compressed position, so that after the compression was removed, the sample is unable to fully bounce back. Among all aging conditions, accelerated aging at high temperatures results in the greatest compression. When comparing UVT and UV samples, UV samples, which are the samples that were under-cured, exhibited greater degree of compression than the UVT samples.

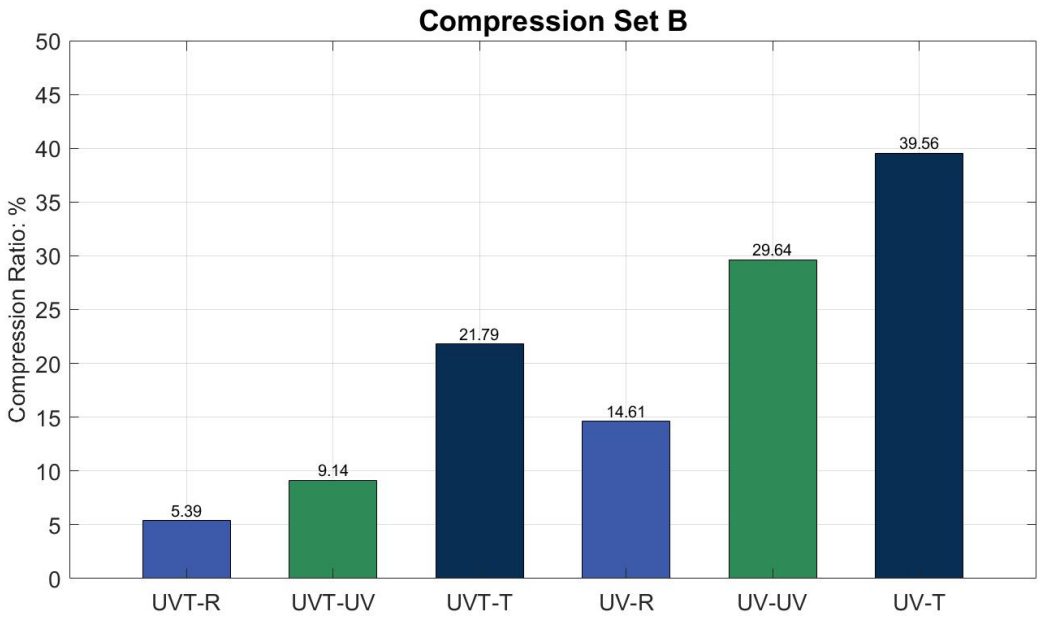

Figure 7 Compression ratio of the tested samples

3.4 Change of Color

Figure 8**Error! Reference source not found.** shows coloration across different curing and aging conditions. Freshly cured material was colorless and semi-opaque. Room temperature aged samples exhibited almost no yellowing, while aged material, especially UV exposed samples, was notably yellowed. Yellowing may be a result of oxidation to the UV-sensitizer, 9,10-diethoxyanthracene. Alternatively, yellowing in silicones is known to be caused by the formation of colloidal platinum particles following hydrosilylation (Lewis, Lewis, & Uriarte, 1992). The most significant yellowing was observed from silicones cured only via UV. UV group samples exhibited the lowest degree of functional group conversion immediately after curing, with a significant number of Si-H groups and vinyl groups remaining in the polymer matrix. With additional low-intensity UV illumination, the catalyst was activated and continued to catalyze the crosslinking process. The colloidal platinum particles were trapped in the fully crosslinked matrix after 6 to 8 weeks of UV aging, scattering light and rendering the silicone yellow. For any

applications that are sensitive to optical transparency, the printed part must be thermally post-cured. Otherwise, any additional UV illumination must be prohibited to ensure optical transparency, which could limit the application of the material.

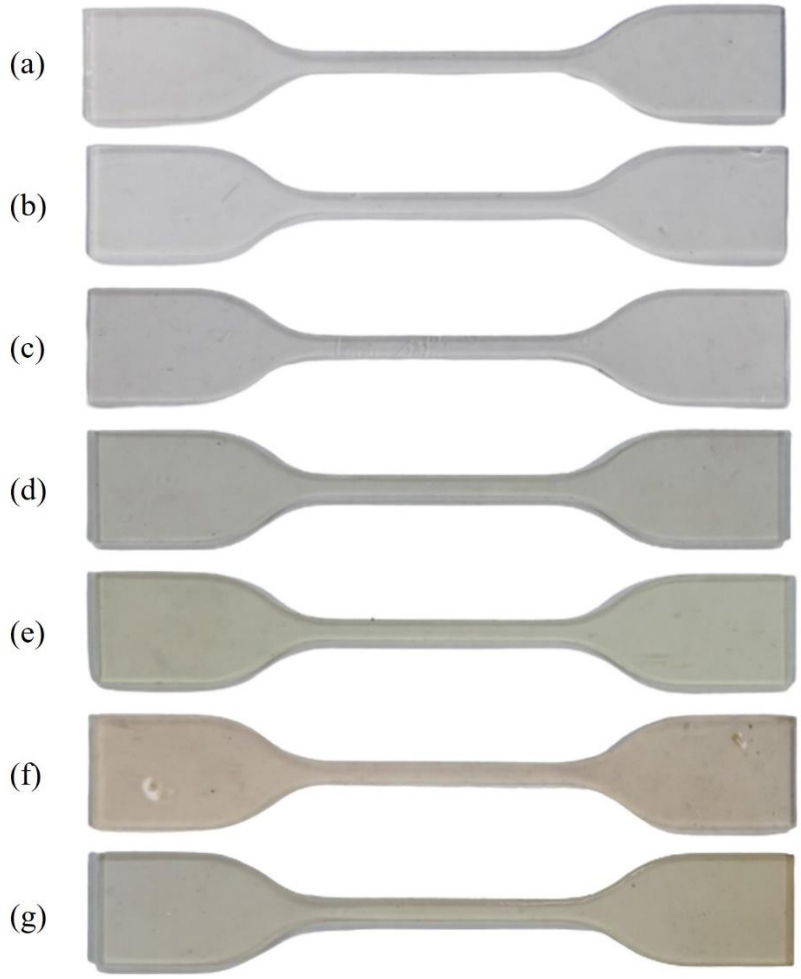

Figure 8 Tensile samples color comparison (a) UV green body (b) UVT green body (c) UVT_thermally-aged for 3 weeks (d) UVT_UV-aged for 8 weeks (e) UV_UV-aged for 4 weeks (f) UV_UV-aged for8 weeks (g) UV_thermally-aged for 4 weeks

4. Conclusion

In this paper, the aging behavior of a Pt-catalyzed, UV-curable PDMS was investigated. The results show that UV treatment alone results in under-cured material, and subsequent exposure to either additional UV or elevated temperatures (i.e. thermal aging) causes the material slowly

evolve as a it reaches a finally cured state over the course of a few weeks. UV cured samples that underwent subsequent post-curing at 135 ^{o}C exhibited minimal changes to tensile properties (i.e. strength, elongation, modulus) under by UV and thermal aging conditions. For samples that are UV cured only, the tensile strength increases as the polymer continues to crosslink, then stabilizes when the polymer is fully crosslinked. For any application that is sensitive to creep or optical transparency, post-curing is necessary to reduce creep and prevent yellowing. With the help of FTIR spectroscopy, no new chemical bonds were detected, which may imply that no chain scission or thermal degradation occurs in the polymer matrix. This PDMS formulation exhibits very good aging properties over time.

Future work includes exploring the thermal aging behavior under higher temperatures. Higher temperatures (greater than 250 °C) not only accelerate the crosslinking rate but also involve additional chemical reactions such as oxidation, resulting in possible loss of mass, further increase in modulus and decrease in elongation. Further experiments are needed to identify these chemical reactions and their effects on the mechanical properties.

Acknowledgment

This work was performed under the auspices of the U.S. Department of Energy by Lawrence Livermore National Laboratory (LLNL) under Contract DE-AC52-07NA27344. IM number: LLNL-JRNL-840405.

Reference

Al-Turaif, H. A. (2010). Effect of nano TiO2 particle size on mechanical properties of cured epoxy resin. *Progress in Organic Coatings, 69*(3), 241-246.

Bhagat, A. A., Jothimuthu, P., & Papautsky, I. (2007). Photodefinable polydimethylsiloxane (PDMS) for rapid lab-on-a-chip prototyping. *Lab Chip, 7*(9), 1192-1197. doi:10.1039/b704946c

Cai, C., Miller, D. C., Tappan, I. A., Dauskardt, R. H. J. S. E. M., & Cells, S. (2016). Degradation of thermally-cured silicone encapsulant under terrestrial UV. *Solar Energy Materials and Solar Cells, 157*, 346-353.

Cong, H., & Pan, T. J. A. F. M. (2008). Photopatternable conductive PDMS materials for microfabrication. *Advanced Functional Materials, 18*(13), 1912-1921.

Dendukuri, D., Panda, P., Haghgooie, R., Kim, J. M., Hatton, T. A., & Doyle, P. S. J. M. (2008). Modeling of oxygen-inhibited free radical photopolymerization in a PDMS microfluidic device. *Macromolecules, 41*(22), 8547-8556.

Eddington, D. T., Puccinelli, J. P., & Beebe, D. J. (2006). Thermal aging and reduced hydrophobic recovery of polydimethylsiloxane. *Sensors and Actuators B: Chemical, 114*(1), 170-172.

Fry, B. E., & Neckers, D. J. M. (1996). Rapid photoactivated hydrosilation polymerization of vinyldimethylsilane. *Macromolecules, 29*(16), 5306-5312.

Hanu, L. G., Simon, G. P., Cheng, Y.-B. J. P. d., & stability. (2006). Thermal stability and flammability of silicone polymer composites. *Polymer Degradation and Stability, 91*(6), 1373-1379.

Hayashi, T., & Yamasaki, K. (2007). C–E bond formation through asymmetric hydrosilylation of alkenes. *Comprehensive Organometallic Chemistry III, 10*, 815-838.

Holländer, J., Hakala, R., Suominen, J., Moritz, N., Yliruusi, J., & Sandler, N. J. I. j. o. p. (2018). 3D printed UV light cured polydimethylsiloxane devices for drug delivery. *International journal of pharmaceutics, 544*(2), 433-442.

Hopf, R., Bernardi, L., Menze, J., Zündel, M., Mazza, E., & Ehret, A. E. J. J. o. t. m. b. o. b. m. (2016). Experimental and theoretical analyses of the age-dependent large-strain behavior of Sylgard 184 (10: 1) silicone elastomer. *Journal of the mechanical behavior of biomedical materials, 60*, 425-437.

Kaneko, T., Ito, S., Minakawa, T., Hirai, N., Ohki, Y. J. P. D., & Stability. (2019). Degradation mechanisms of silicone rubber under different aging conditions. *Polymer Degradation and Stability, 168*, 108936.

Lewis, L. N., Lewis, N., & Uriarte, R. J. (1992). Hydrosilylation: A" Homogeneous" Reaction Really Catalyzed by Colloids. In: ACS Publications.

Liravi, F., & Toyserkani, E. J. A. M. (2018). Additive manufacturing of silicone structures: A review and prospective. *Additive Manufacturing, 24*, 232-242.

Liu, G., Kaspar, J., Reinold, L. M., Graczyk-Zajac, M., & Riedel, R. J. E. A. (2013). Electrochemical performance of DVB-modified SiOC and SiCN polymer-derived negative electrodes for lithium-ion batteries. *Electrochimica Acta, 106*, 101-108.

Liu, M., Sun, J., & Chen, Q. (2009). Influences of heating temperature on mechanical properties of polydimethylsiloxane. *Sensors and Actuators A: Physical, 151*(1), 42-45.

Lu, K., & Li, J. J. J. o. t. E. C. S. (2016). Fundamental understanding of water vapor effect on SiOC evolution during pyrolysis. *Journal of the European Ceramic Society, 36*(3), 411-422.

Lukin, R. Y., Kuchkaev, A. M., Sukhov, A. V., Bekmukhamedov, G. E., & Yakhvarov, D. G. J. P. (2020). Platinum-catalyzed hydrosilylation in polymer chemistry. *Polymers, 12*(10), 2174.

Masson, J.-F., Collins, P., Riahinezhad, M., Lopez-Carreon, I., & Johansen, J. J. C. J. o. C. E. (2022). Resistance of a silicone membrane to long-term UV and moisture aging in light of climate change. *Canadian Journal of Civil Engineering, 49*(2), 192-200.

Mata, A., Fleischman, A. J., & Roy, S. J. B. m. (2005). Characterization of polydimethylsiloxane (PDMS) properties for biomedical micro/nanosystems. *Biomedical microdevices, 7*(4), 281-293.

Mayer, T., Burget, D., Mignani, G., & Fouassier, J. J. J. o. P. S. P. A. P. C. (1996). Photohydrosilylation reaction of silicone polymers. Platinum‐based photocatalysts: Trimethyl (β‐dicarbonyl) platinum IV complexes. *Journal of Polymer Science Part A: Polymer Chemistry, 34*(15), 3141-3146.

Munaro, A. P., da Cunha, G. P., Filgueiras, J. G., Pinto, J. M., Munaro, M., de Azevedo, E. R., . . . Stability. (2019). Ageing and structural changes in PDMS rubber investigated by time domain NMR. *Polymer Degradation and Stability, 166*, 300-306.

Murphy, S. V., & Atala, A. J. N. b. (2014). 3D bioprinting of tissues and organs. *Nature biotechnology, 32*(8), 773-785.

Oxman, J. D., & Boardman, L. D. (1992). Radiation activated hydrosilation reaction. In (Vol. U.S. Patent No. 5,145,886.): Washington, DC: U.S. Patent and Trademark Office.

Oxman, J. D., & Boardman, L. D. (2002). Hydrosilation reaction utilizing a (cyclopentadiene)(sigma-aliphatic) platinum complex and a free radical photoinitiator. In (Vol. U.S. Patent No. 6,376,569.): Washington, DC: U.S. Patent and Trademark Office.

Raj M, K., & Chakraborty, S. J. J. o. A. P. S. (2020). PDMS microfluidics: A mini review. *Journal of Applied Polymer Science, 137*(27), 48958.

Rodriguez, N., Ruelas, S., Forien, J.-B., Dudukovic, N., DeOtte, J., Rodriguez, J., . . . Oakdale, J. S. J. P. (2021). 3D printing of high viscosity reinforced silicone elastomers. *Polymers, 13*(14), 2239.

Rodriguez, N. A., Song, H., Chen, M., Oakdale, J. S., Duoss, E. B., Seepersad, C. C., & Crawford, R. H. J. A. M. (2022). Use of wire grid polarizers with liquid crystal display for large-volume stereolithography. *Additive Manufacturing, 52*, 102641.

Schneider, F., Draheim, J., Kamberger, R., & Wallrabe, U. (2009). Process and material properties of polydimethylsiloxane (PDMS) for Optical MEMS. *Sensors and Actuators A: Physical, 151*(2), 95-99.

Shimada, A., Sugimoto, M., Kudoh, H., Tamura, K., Seguchi, T. J. I. T. o. D., & Insulation, E. (2014). Degradation mechanisms of silicone rubber (SiR) by accelerated ageing for cables of nuclear power plant. *IEEE Transactions on Dielectrics and Electrical Insulation, 21*(1), 16-23.

Sirrine, J. M., Meenakshisundaram, V., Moon, N. G., Scott, P. J., Mondschein, R. J., Weiseman, T. F., . . . Long, T. E. J. P. (2018). Functional siloxanes with photo-activated, simultaneous chain extension and crosslinking for lithography-based 3D printing. *Polymer, 152*, 25-34.

Song, H., Rodriguez, N. A., Seepersad, C. C., Crawford, R. H., Chen, M., & Duoss, E. B. J. A. M. (2021). Development of a variable tensioning system to reduce separation force in large scale stereolithography. *Additive Manufacturing, 38*, 101816.

Sycks, D. G., Wu, T., Park, H. S., & Gall, K. J. J. o. A. P. S. (2018). Tough, stable spiroacetal thiol‐ene resin for 3D printing. *Journal of Applied Polymer Science, 135*(22), 46259.

Thrasher, C. J., Schwartz, J. J., Boydston, A. J. J. A. a. m., & interfaces. (2017). Modular elastomer photoresins for digital light processing additive manufacturing. *ACS applied materials & interfaces, 9*(45), 39708-39716.

Tian, K., Bae, J., Bakarich, S. E., Yang, C., Gately, R. D., Spinks, G. M., . . . Vlassak, J. J. J. A. M. (2017). 3D printing of transparent and conductive heterogeneous hydrogel–elastomer systems. *Advanced Materials, 29*(10), 1604827.

Wallin, T., Pikul, J., Bodkhe, S., Peele, B., Mac Murray, B., Therriault, D., . . . Shepherd, R. J. J. o. M. C. B. (2017). Click chemistry stereolithography for soft robots that self-heal. *Journal of Materials Chemistry B, 5*(31), 6249-6255.

Wang, L., Lu, K., & Ma, R. J. A. P. A. (2019). Effects of different polymer precursors on the characteristics of SiOC bulk ceramics. *Applied Physics A, 125*(6), 1-13.

Xi, L., Liu, Z., Su, J., Bei, Y., Xiang, H., & Liu, X. J. J. o. A. P. S. (2019). UV‐activated hydrosilylation of (Me‐Cp) Pt (Me) 3: Enhanced photocatalytic activity, polymerization kinetics, and photolithography. *Journal of Applied Polymer Science, 136*(47), 48251.

Xiang, H., Wang, X., Ou, Z., Lin, G., Yin, J., Liu, Z., . . . Liu, X. J. P. i. O. C. (2019). UV-curable, 3D printable and biocompatible silicone elastomers. *Progress in Organic Coatings, 137*, 105372.

Xiang, K., Huang, G., Zheng, J., Wang, X., xian Li, G., & Huang, J. (2012). Accelerated thermal ageing studies of polydimethylsiloxane (PDMS) rubber. *Journal of Polymer Research, 19*(5), 1-7.

Xiao, C., Tan, Y., Yang, X., Xu, T., Wang, L., & Qi, Z. (2018). Mechanical properties and strengthening mechanism of epoxy resin reinforced with nano-SiO2 particles and multi-walled carbon nanotubes. *Chemical Physics Letters, 695*, 34-43.

Yang, H., He, Y., Tuck, C., Wildman, R., Ashcroft, I., Dickens, P., & Hague, R. (2013). *High viscosity jetting system for 3D reactive inkjet printing.* Paper presented at the 2013 International Solid Freeform Fabrication Symposium.

Zheng, S., Zlatin, M., Selvaganapathy, P. R., & Brook, M. A. J. A. M. (2018). Multiple modulus silicone elastomers using 3D extrusion printing of low viscosity inks. *Additive Manufacturing, 24*, 86-92.